











Unrestrained cleavage of Roquin-1 by MALT1 induces spontaneous T cell activation and the development of autoimmunity

Henrik Schmidt^{a,1}, Timsse Raj^{a,1} , Thomas J. O'Neill^b, Andreas Muschwack^c, Florian Giesert^d , Arlinda Negraschus^a , Kai P. Hoefig^e, Gesine Behrens^a, Lena Esser^a, Christina Baumann^e, Regina Feederle^f , Carlos Plaza-Sirvent^g, Arie Geerlof^h , Andreas Gewies^b, Sophie E. Isayⁱ , Jürgen Ruland^{h,j}, Ingo Schmitz^g , Wolfgang Wurst^{d,k,l}, Thomas Korn^{c,m} , Daniel Krappmann^b , and Vigo Heissmeyer^{a,e,2}

Edited by Tak Mak, University of Toronto, Toronto, ON, Canada; received June 7, 2023; accepted October 2, 2023

Constitutive activation of the MALT1 paracaspase in conventional T cells of *Malt1*^{TBM/TBM} (TRAF6 Binding Mutant = TBM) mice causes fatal inflammation and autoimmunity, but the involved targets and underlying molecular mechanisms are unknown. We genetically rendered a single MALT1 substrate, the RNA-binding protein (RBP) Roquin-1, insensitive to MALT1 cleavage. These *Rc3h1*^{Mins/Mins} mice showed normal immune homeostasis. Combining *Rc3h1*^{Mins/Mins} alleles with those encoding for constitutively active MALT1 (TBM) prevented spontaneous T cell activation and restored viability of *Malt1*^{TBM/TBM} mice. Mechanistically, we show how antigen/MHC recognition is translated by MALT1 into Roquin cleavage and derepression of Roquin targets. Increasing T cell receptor (TCR) signals inactivated Roquin more effectively, and only high TCR strength enabled derepression of high-affinity targets to promote Th17 differentiation. Induction of experimental autoimmune encephalomyelitis (EAE) revealed increased cleavage of Roquin-1 in disease-associated Th17 compared to Th1 cells in the CNS. T cells from *Rc3h1*^{Mins/Mins} mice did not efficiently induce the high-affinity Roquin-1 target IκB_{NS} in response to TCR stimulation, showed reduced Th17 differentiation, and *Rc3h1*^{Mins/Mins} mice were protected from EAE. These data demonstrate how TCR signaling and MALT1 activation utilize graded cleavage of Roquin to differentially regulate target mRNAs that control T cell activation and differentiation as well as the development of autoimmunity.

autoimmunity | antigen receptor signaling | T cell differentiation | RNA-binding protein | paracaspase

Antigen recognition by T cells activates MALT1, and the scaffold function of MALT1 induces JNK/AP-1 and IKK/NF-κB signal transduction (1). Simultaneously, MALT1 paracaspase function is activated to cleave specific target proteins (2). Up to now, 30 protein substrates have been predicted to be cleaved by MALT1, and cleavage of almost 20 proteins has been confirmed in cleavage assays (3). Substrates include regulators of NF-κB signal transduction like RELB, CYLD, HOIL, BCL10, TNFAIP3, and MALT1 itself (1). Another set of targets are RNA-binding proteins (RBPs) like Roquin-1, Roquin-2, Regnase-1, Regnase-2, Regnase-4, and N4BP1 (3–6). Recently, additional proteins including TAB3, CASP10, CILK1, ILDR2, and TANK were predicted to harbor candidate cleavage sites and were tested for being potential targets (3). Interestingly, genetic manipulation in mice causing either loss-of-function or constitutive activation of the MALT1 paracaspase induced inflammatory or autoimmune disease (7–10). At this point, it is unclear whether deregulation of NF-κB or the posttranscriptional regulators drive the observed phenotypes. Furthermore, these phenotypes could relate to unknown targets and involve deregulation of single or multiple targets.

Posttranscriptional gene regulation exerts essential control over immune responses. In fact, human patients as well as mouse models with hypomorphic mutations in the *Rc3h1* gene develop severe autoimmune or inflammatory diseases (11, 12). The *Rc3h1* encoded RNA-binding protein Roquin-1 and its paralog Roquin-2 work redundantly in T cells (13) and decrease mRNA stability or translation efficiency of their targets including *Icos*, *Irf4*, *Tnfrsf4* (*Ox40*), *Tnf*, and *Nfkbid* (IκB_{NS}) (13–16). These targets are recognized through the amino-terminal ROQ domain, which binds with high affinity to a well-defined constitutive decay element (CDE), originally identified in the *Tnf* 3'-UTR (15, 17–21). The ROQ domain also interacts with CDE-like elements of a relaxed consensus, with U-rich stem-loop structures and alternative decay elements (ADE), as well as with the low-affinity linear binding elements (LBE) (14, 22, 23). While the amino-terminus of Roquin interacts with RNA, the carboxy-terminus recruits the CCR4–NOT complex to induce target mRNA

Significance

We show that autoimmunity, caused by conventional T cells expressing constitutively active MALT1 paracaspase, is triggered by cleavage of a single substrate, the RNA-binding protein Roquin-1. MALT1 translates graded TCR signal strength into binary cell fate decisions, as decreasing Roquin activities are associated with differential derepression of low- and high-affinity targets. As an example of this regulation, we find that Th17 differentiation requires high TCR strength, strongly reduced Roquin activity and the concomitant induction of the modulator of transcription, IκB_{NS}, a high-affinity Roquin target. Together, we show that interfering with a distinct TCR strength integrating signaling pathway selectively mitigates T cell-driven immunopathology.

Author contributions: H.S., T.R., F.G., A.N., T.K., D.K., and V.H. designed research; H.S., T.R., T.J.O., A.M., A.N., K.P.H., G.B., L.E., C.B., and C.P.-S. performed research; T.J.O., F.G., R.F., A. Geerlof, A. Gewies, S.E.I., J.R., I.S., W.W., T.K., and D.K. contributed new reagents/analytic tools; H.S., T.R., T.J.O., A.M., T.K., D.K., and V.H. analyzed data; and T.R., H.S. and V.H. wrote the paper.

The authors declare no competing interest.

This article is a PNAS Direct Submission.

Copyright © 2023 the Author(s). Published by PNAS. This open access article is distributed under [Creative Commons Attribution-NonCommercial-NoDerivatives License 4.0 \(CC BY-NC-ND\)](https://creativecommons.org/licenses/by-nc-nd/4.0/).

¹H.S. and T.R. contributed equally to this work.

²To whom correspondence may be addressed. Email: vigo.heissmeyer@med.uni-muenchen.de.

This article contains supporting information online at <https://www.pnas.org/lookup/suppl/doi:10.1073/pnas.2309205120/-/DCSupplemental>.

Published November 21, 2023.

deadenylation and degradation (11, 15, 24, 25). Complete loss of Roquin-1 expression causes perinatal lethality, while combined conditional ablation of Roquin-1 and Roquin-2 encoding alleles in T cells leads to aberrant T cell activation and differentiation. In these mice, excessive T follicular helper (Tfh) and Th17 differentiation were observed (4, 13, 26). In T cells, the TCR-activated paracaspase MALT1 cleaves Roquin-1 and Roquin-2 and separates RNA-binding and CCR4-NOT recruitment functions (4). The MALT1 paracaspase is critical for Th17 differentiation, and *Malt1*^{PM/PM} (C472A paracaspase mutant) mice are less susceptible to experimentally induced autoimmune encephalomyelitis (EAE) (8, 10). Surprisingly, *Malt1*^{PM/PM} mice suffer from spontaneous IFN γ -mediated autoinflammation as well as an IPEX (immunodysregulation polyendocrinopathy enteropathy X-linked)-like imbalance of increased T effector (Teff) to Treg cell ratios (8–10, 27, 28). On the other hand, mutations of the TRAF6 binding sites in MALT1 were associated with unrestrained constitutive paracaspase activity, while TCR-induced and TRAF6/MALT1-dependent NF- κ B activation was blocked (7). *Malt1*^{TBM/TBM} (TBM = TRAF6 Binding Mutant) mice die within the first three weeks of life and showed spontaneous T cell activation and multiorgan infiltration of leukocytes, and this autoimmune/autoinflammatory disease involved MALT1 activity in conventional T cells (7).

Thymocyte selection has been shown to depend on T cell receptor (TCR) signal strength (29, 30). In peripheral T cells, stronger TCR signals have been proposed to promote Th1 over Th2 or Th17 over Treg fates, and variable results have been reported with respect to Th1 over Tfh cell fate decisions (31–35). Only few reports have provided a mechanistic understanding of how TCR-peptide:MHC-II affinities are translated into differential gene expression (33, 36), and the molecules and mechanisms that can translate graded TCR signal strengths into binary cell fate decisions are mostly unknown.

Here, we show that MALT1-insensitive Roquin-1 alleles rescued fatal autoimmunity in mice with constitutively active MALT1. Strong TCR signals were needed to sufficiently decrease the activity of Roquin and enable expression of its high-affinity target *Nfkbid*/I κ B_{NS}, which is required for Th17 differentiation. Indeed, Roquin-1 cleavage was critical for Th17 cell-driven immunopathology since mice expressing MALT1-insensitive Roquin-1 were protected from EAE.

Results

Continuous Roquin-1 Cleavage Triggers Autoimmunity. Recently, mutations in MALT1 that block the TRAF6 binding motifs (T6BM) were shown to inactivate antigen-receptor-induced NF- κ B activation. At the same time, these mutations rendered the MALT1 protease constitutively active. These mice developed autoimmunity, and showed leukocyte infiltration into multiple tissues and inflammation, for which the MALT1 activity in conventional T cells was found responsible (7). To determine the importance of signal-induced cleavage of Roquin-1, we created a MALT1-insensitive allele (*Rc3h1*^{Mins}) by CRISPR/Cas9 genome editing in the mouse germline. We introduced two point mutations in exons 10 and 11 through homology-directed repair exchanging arginine 510 and arginine 579 to alanine (SI Appendix, Fig. S1A). The mutations blocked the main as well as alternative MALT1 cleavage sites of Roquin-1 (4), as confirmed in immunoblots of Th1 cells from *Rc3h1*^{Mins/Mins} mice stimulated with PMA and ionomycin (P/I) but did not affect cleavage of Regnase-1 (SI Appendix, Fig. S1B). The founder and all backcrossed *Rc3h1*^{Mins/+} or *Rc3h1*^{Mins/Mins} mice appeared normal and showed

normal thymocyte development (SI Appendix, Fig. S1C). There was a small reduction in thymic Treg cell (CD4-SP; Foxp3⁺) frequencies, which was not significant in absolute numbers as there were slightly more thymocytes in *Rc3h1*^{Mins/Mins} compared to wild-type mice (SI Appendix, Fig. S1D). Peripheral Treg cells of *Rc3h1*^{Mins/Mins} mice were not reduced (SI Appendix, Fig. S1E), and *Rc3h1*^{Mins/Mins} mice did not show activation of peripheral CD4⁺ or CD8⁺ T cells (SI Appendix, Fig. S1F).

To detect Roquin-1 cleavage on the single-cell level, we generated a monoclonal antibody that does not recognize full-length Roquin-1 but specifically binds the free carboxy-terminus of truncated Roquin-1 (aa 1-510) or Roquin-2 (aa 1-509), which arise due to MALT1-dependent cleavage (SI Appendix, Fig. S2A–C). Importantly, the 20G6 hybridoma supernatant was able to detect the P/I-induced cleavage of endogenous Roquin protein in immunoblots of extracts from stimulated wild-type but not *Rc3h1*^{Mins/Mins} thymocytes (SI Appendix, Fig. S2D). We validated this antibody further by intracellular staining and flow cytometry showing increased cleavage of Roquin after P/I stimulation of WT thymocytes as compared to unstimulated controls (SI Appendix, Fig. S2E) or stimulated thymocytes from *Rc3h1*^{Mins/Mins} (SI Appendix, Fig. S2F) or *Malt1*^{-/-} genotypes (SI Appendix, Fig. S2G). Using recombinant mouse I κ B_{NS} protein, we also generated a monoclonal antibody against this target of Roquin. The 4C1 hybridoma supernatant worked in immunoblots and flow cytometry and detected transfected mouse I κ B_{NS} (SI Appendix, Fig. S2H) or PMA-induced endogenous I κ B_{NS} protein in lymphocytes from wild-type but not *Nfkbid*^{-/-} mice (SI Appendix, Fig. S2I) and in P/I-stimulated A20 B cells (SI Appendix, Fig. S2J) or OVA₃₂₃₋₃₃₉-stimulated OTII T cells (SI Appendix, Fig. S2K).

To determine whether phenotypes arising due to constitutive MALT1 protease activity depended on the cleavage of Roquin-1, we combined *Malt1*^{TBM/TBM} with *Rc3h1*^{Mins/Mins} alleles. We confirmed constitutive proteolytic activity of MALT1 by detecting the aa1-510 cleavage product of Roquin in immunoblots of extracts from unstimulated lymph node cells of *Malt1*^{TBM/TBM} mice and showed that this specific signal was undetectable in controls from WT, *Rc3h1*^{Mins/Mins} or *Malt1*^{TBM/TBM}; *Rc3h1*^{Mins/Mins} mice (Fig. 1A). The Roquin target I κ B_{NS} was strongly induced in cells from *Malt1*^{TBM/TBM} mice, which was abolished by combined *Rc3h1*^{Mins/Mins} alleles (Fig. 1A). Single-cell analysis showed that Roquin, also in CD4⁺ T cells from *Malt1*^{TBM/TBM} mice, exhibited constitutive cleavage (Fig. 1B).

The combination with homozygous alleles encoding for MALT1-insensitive Roquin-1 fully rescued mortality in all *Malt1*^{TBM/TBM}; *Rc3h1*^{Mins/Mins} mice. In contrast, *Malt1*^{TBM/TBM} or *Malt1*^{TBM/TBM}; *Rc3h1*^{+ /Mins} mice had to be killed between day 17 and day 20 of life because of their severe burden, and only one *Malt1*^{TBM/TBM} *Rc3h1*^{+ /Mins} mouse survived (Fig. 1C). Consistent with restored viability in *Malt1*^{TBM/TBM}; *Rc3h1*^{Mins/Mins} mice we found slightly reduced spleen sizes, no rescue of splenocyte numbers (Fig. 1D) but significantly reduced frequencies and numbers of activated T cells as determined by CD3⁺CD69⁺ measurements (Fig. 1E), as well as a partial rescue in frequencies of effector memory T cells as compared to *Malt1*^{TBM/TBM} mice (Fig. 1F).

The upregulation of Roquin targets in T cells from *Malt1*^{TBM/TBM} mice was prevented in T cells from *Malt1*^{TBM/TBM}; *Rc3h1*^{Mins/Mins} mice as shown for I κ B_{NS} (Fig. 1G) and Ox40, IRF4, and ICOS (Fig. 1H and SI Appendix, Fig. S1G).

Together, these data show that cleavage of Roquin-1 and Roquin-2 and derepression of Roquin targets can be detected on the single-cell level. Inactivating Roquin-1 cleavage does not

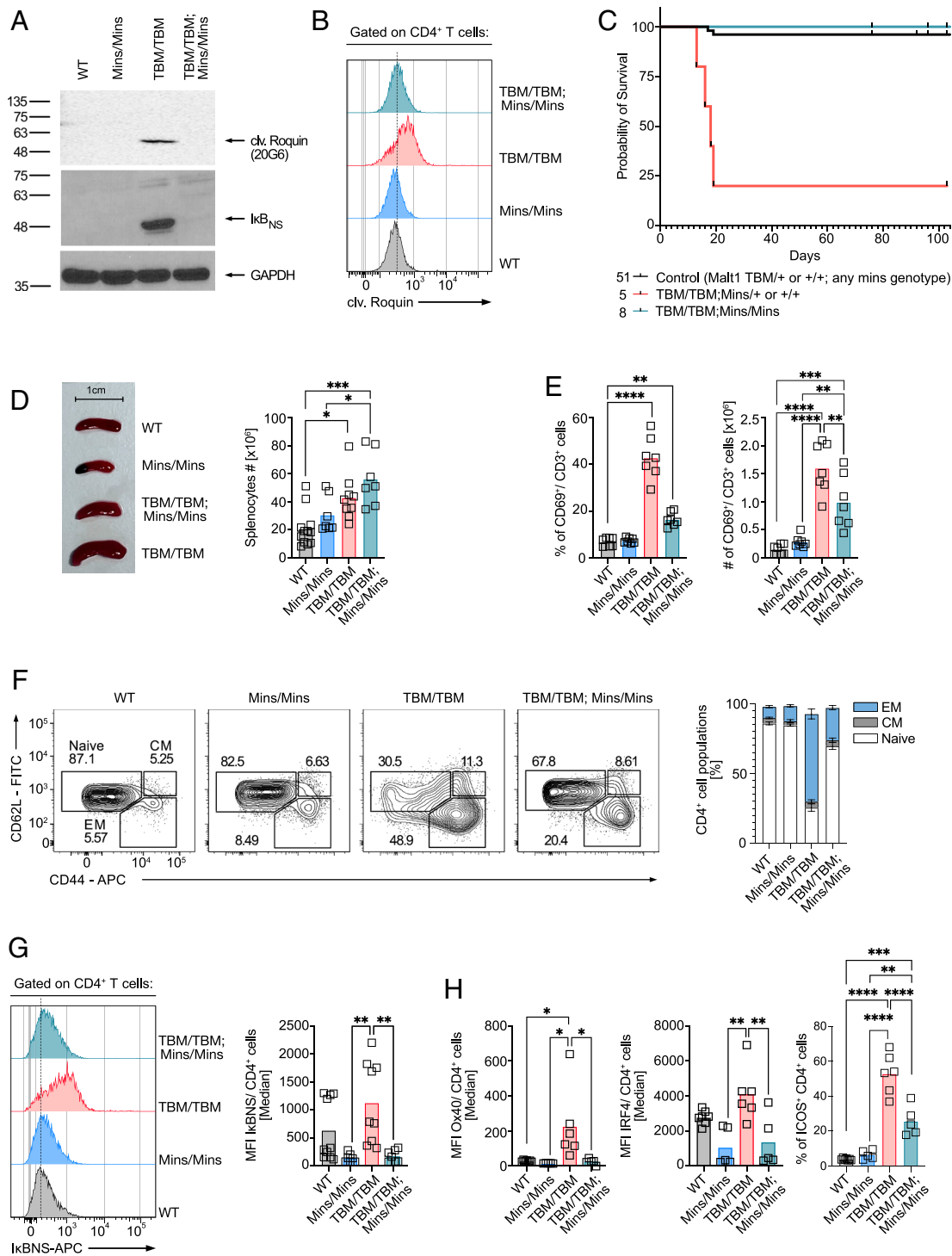


Fig. 1. Continuous Roquin cleavage leads to autoimmunity. (A) Western blot analysis of protein extracts taken from total lymph node cells of WT, *Rc3h1*^{Mins/Mins} (Mins/Mins), *Malt1*^{TBM/TBM} (TBM/TBM), and combined *Malt1*^{TBM/TBM}; *Rc3h1*^{Mins/Mins} (TBM/TBM; Mins/Mins) mice. Spontaneous Roquin cleavage and upregulation of IκB_{NS} is prevented in TBM/TBM; Mins/Mins mice. (B) Representative flow cytometry analysis of Roquin cleavage pregated on CD4⁺ T cells (*n* = 6–10). (C) Kaplan-Meier plot showing survival of WT, TBM/TBM, and TBM/TBM; Mins/Mins mice (*n* = 5–51). Combining Malt1-insensitive Roquin-1 rescues survival of mice with constitutive MALT1 activity. (D) Representative spleen sizes and quantification of spleen weights and numbers of splenocytes. (E) Quantification of frequencies and numbers of CD69⁺ CD3⁺ cells in spleens. (F) Representative plots and quantifications of peripheral CD4⁺ T cell activation from spleens of WT, Mins/Mins, TBM/TBM and TBM/TBM; Mins/Mins mice showing naive (CD62L^{hi} CD44⁻), central memory (CD62L^{hi} CD44⁺), and effector memory (CD62L^{low} CD44⁺) T cells (*n* = 6–10). (G) Representative plot and quantification of the direct Roquin target IκB_{NS} in splenic CD4⁺ T cells (*n* = 6–10). (H) Quantification of the direct Roquin target expression Ox40, IRF4, or ICOS expression in splenic CD4⁺ T cells, respectively (*n* = 6–10). Error bars represent mean ± SEM. CM: central memory, EM: effector memory, MFI: median fluorescence intensity. Statistical analysis was performed using one-way ANOVA with Dunnett's post hoc test. **P* < 0.05, ***P* < 0.01, ****P* < 0.001, and *****P* < 0.0001.

have an obvious impact in the absence of challenge. However, constitutive Roquin-1 cleavage leads to spontaneous activation of T cells, T cell effector function, and the development of autoimmunity.

Cleavage of Roquin by MALT1 Is Correlated with TCR Signal Strength. We aimed to correlate Roquin cleavage to T cell responses by analyzing cleavage of Roquin in ex vivo stimulated CD4⁺ T cells. We found no Roquin cleavage in cells with

low CD69 expression (Fig. 2A). We also addressed whether the strength of the TCR signal during stimulation of T cells correlated with the extent of Roquin cleavage. Using CD4⁺ T cells stimulated with a constant amount of anti-CD28 (10 μg/mL), we found that increasing agonistic anti-CD3 doses (0.01–0.15 μg/mL) lead to an expected increase in CD69 expression, and similarly increased the MALT1-cleaved Roquin (20G6) signal (Fig. 2A and B) and IκB_{NS} expression (SI Appendix, Fig. S3A). To determine Roquin cleavage in T cells recognizing antigen, we tested OT-II T cells stimulated with cognate OVA₃₂₃₋₃₃₉ peptide loaded splenocytes. Cleavage of Roquin and upregulation of IκB_{NS} occurred in a concentration-dependent manner and correspondingly increased in the range of 0.1–10.0 μg/mL OVA antigen (SI Appendix, Fig. S3B and C), while CD69 upregulation showed stronger increases already at lower concentrations (SI Appendix, Fig. S3D). We also tested a mutated OVA₃₂₃₋₃₃₉ peptide replacing histidine 331 with arginine (OVA_{R9}), which is known to have a lower functional avidity for activating OT-II TCR transgenic T cells, requiring about 10-fold higher effective

concentrations in proliferation experiments (4, 37, 38). This peptide was less efficient in inducing Roquin cleavage or CD69 and IκB_{NS} expression in CD25⁺ T cells at concentrations that elicited maximal responses for wild-type antigen (SI Appendix, Fig. S3E and F).

Together, these data show that antigen density and the strength of the TCR signal stimulate graded MALT1-mediated cleavage of Roquin.

Roquin Targets Exhibit Different Functional Avidities. We then asked whether increasing doses of antigen and concomitantly decreased Roquin activity differentially affected Roquin targets. We focused on IκB_{NS} (*Nfkbid*) and Ox40 (*Tnfrsf4*) in OT-II T cells stimulated with antigen doses ranging from 0.01 to 10 μg/mL OVA₃₂₃₋₃₃₉ (Fig. 2C). We found Ox40 expression fully induced at 0.1 μg/mL OVA antigen (Fig. 2C and D), while maximum responses of IκB_{NS} required at least 10-fold higher concentrations, similar to CD69 (Fig. 2C and D). The 3'-UTR of *Nfkbid* harbors 6 stem-loop structures and two of these motifs are prototypic

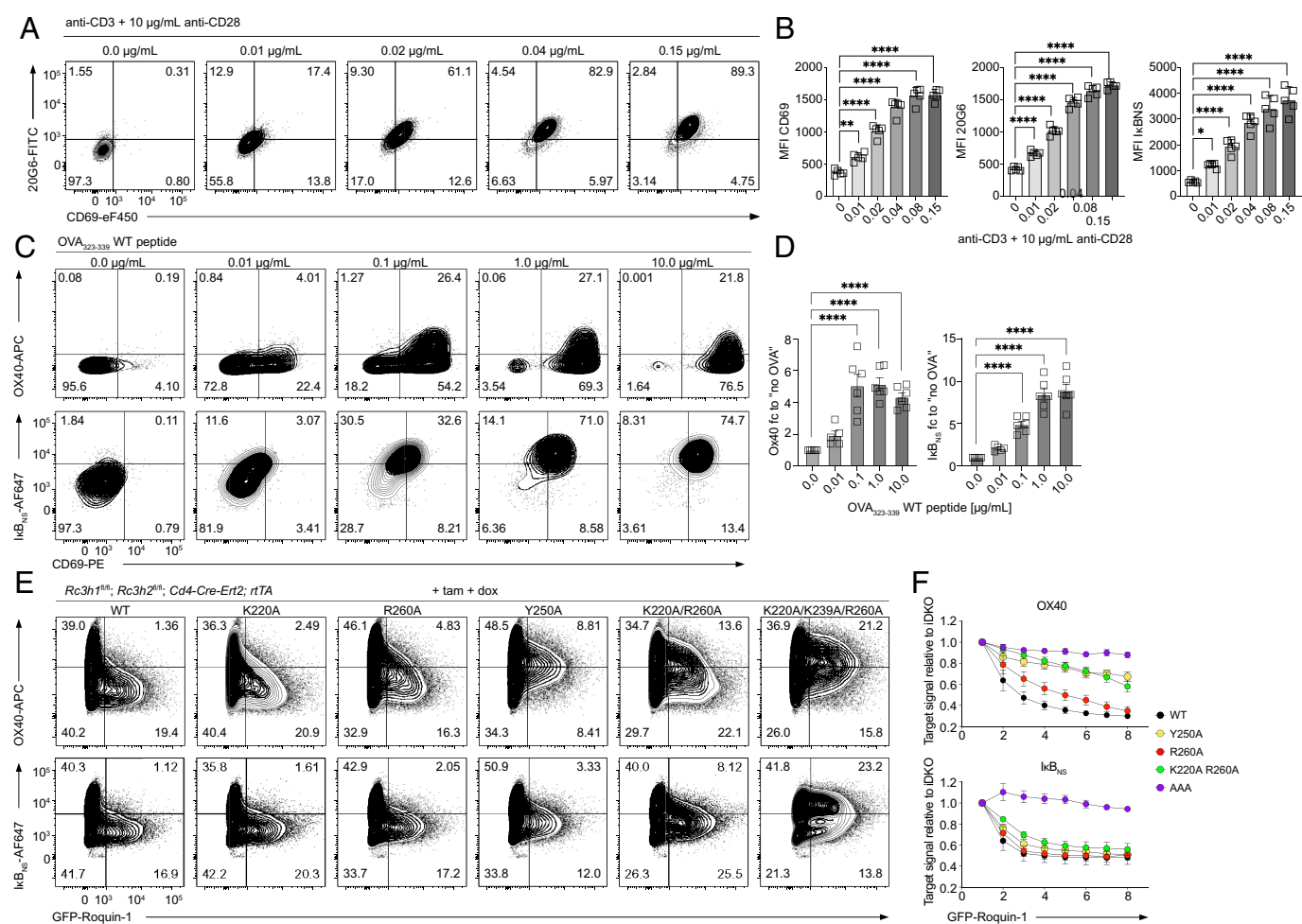


Fig. 2. Correlating Roquin cleavage and target derepression with TCR strength. (A) Representative plots and (B) quantification of Roquin cleavage (20G6) and CD69 expression in T cells stimulated with the indicated anti-CD3 and fixed anti-CD28 (10 μg/mL) concentrations for 18 h. (B) Quantifications display MFI (median fluorescence intensity) of CD69, cleaved Roquin (20G6), and IκB_{NS} (4C1) ($n = 5$). Data presented as mean \pm SD. Statistical analysis was performed using an unpaired Student's t test, two-tailed. * $P < 0.05$, ** $P < 0.01$, *** $P < 0.001$, and **** $P < 0.0001$. (C) In vitro coculture of naive WT OT-II CD4⁺ T cells with OVA₃₂₃₋₃₃₉ peptide-loaded bone marrow derived dendritic cells (BMDCs) for 18 h followed by flow cytometry to detect Ox40 and IκB_{NS} (4C1) expression for OT-II T cells (pregated on $\alpha_V\alpha_2/\beta_5^+$ TCR). Ox40, IκB_{NS} (4C1), and surface CD69 expression were analyzed in stimulations with increasing concentrations of WT OVA₃₂₃₋₃₃₉ peptide. (D) Quantification of Roquin target expression in OT-II T cells from cocultures shown in C, depicting the fold change (fc) in gMFI values of Ox40 or IκB_{NS} (4C1) after stimulation in comparison to unstimulated cells. Data are presented as mean \pm SEM ($n = 3-6$). (E) Representative plots of Ox40 and IκB_{NS} (4C1) expression in iDKO CD4⁺ T cells retrovirally reconstituted with WT or mutant GFP-Roquin-1 constructs. (F) Relative quantification of target expression as in (E) in GFP⁺ cells and within 7 equal-sized gates corresponding to increasing GFP-Roquin-1 expression. WT and mutant GFP-Roquin-1 constructs are color-coded, and individual gMFI values (per target) were normalized to maximum levels observed in iDKO CD4⁺ T cells without retroviral transduction. Data are presented as mean \pm SEM ($n = 3-4$). Statistical analysis was performed using one-way ANOVA with Dunnett's post hoc test. * $P < 0.05$, ** $P < 0.01$, *** $P < 0.001$, and **** $P < 0.0001$.

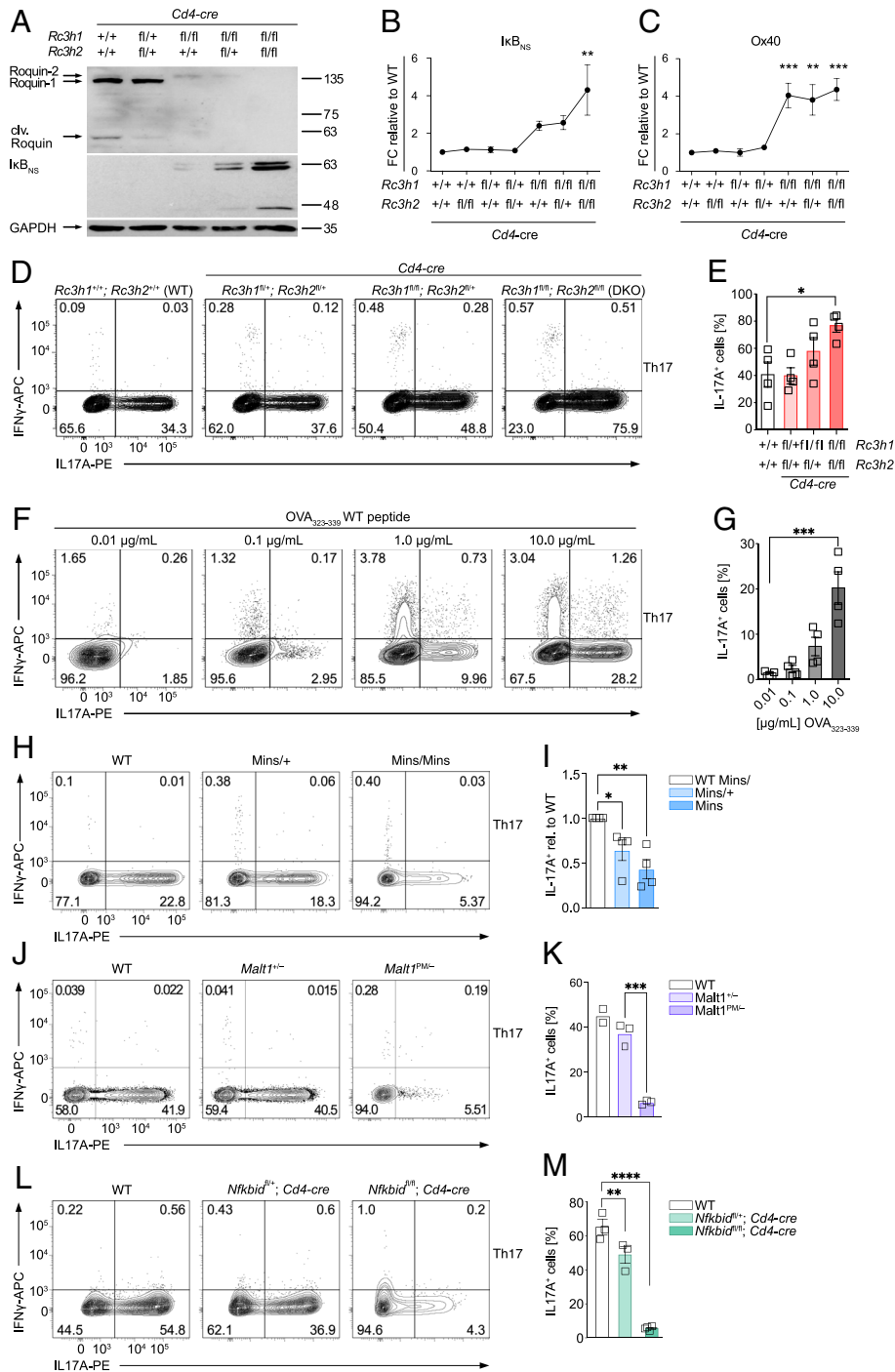
high-affinity CDEs (14, 15, 18), while the 3'-UTR of *Tnfrsf4* has one ADE and one CDE-like stem-loop only, and both of them have lower affinity as compared to a CDE (13, 22, 39). We hypothesized that the molecular basis for the differential derepression lies in the encoded binding site affinities of target mRNAs for the RNA-binding domain of Roquin. To test this, we mutated residues in the ROQ domain of Roquin-1 (K220A, K239A, Y250A and R260A), which are known to contribute to the binding to CDE-, ADE-, and LBE-type motifs (14, 18, 22). We used tamoxifen-inducible double knockout (iDKO) of Roquin-1 and Roquin-2 encoding alleles in CD4⁺ T cells (22, 40, 41) (*SI Appendix, Fig. S4A*) and transduced these T cells with doxycycline-inducible retroviral expression vectors to analyze reconstitution with wild-type or mutant Roquin-1 proteins fused to GFP (11, 22) (*SI Appendix, Fig. S4B*). The mutant proteins were expressed equally well compared to wild-type GFP-Roquin-1, and they fully or partially retained the ability to repress all or some target mRNAs (Fig. 2 *E* and *F* and *SI Appendix, Fig. S4C*). We analyzed target expression by flow cytometry in intervals of increasing GFP expression, normalized to target levels in GFP-negative iDKO cells (*SI Appendix, Fig. S4B*). As expected, reconstitution with wild-type Roquin-1 was most effective to repress targets and the triple alanine mutant (K220A; K239A; R260A) was least effective (Fig. 2 *E* and *F*), since targets like Ox40 and IκB_{NS} did not respond to the GFP-marked expression of the triple alanine mutant. Consistent with the Y250A mutation being selectively involved in the interaction with ADE-type stem-loops as found in the *Tnfrsf4* (Ox40) 3'-UTR (22), this mutant was almost inactive to repress Ox40 but fully active to repress IκB_{NS} (Fig. 2 *E* and *F*). The double-mutant K220; R260A important for ADE- and CDE-type stem-loops (18, 22) discriminated between different targets as it was almost inactive to repress Ox40, while fully active to repress IκB_{NS} (Fig. 2 *E* and *F*). Other targets of Roquin-1, including ICOS and Regnase-1, exhibited an intermediate responsiveness as compared to the differential regulation of Ox40 or IκB_{NS} (Fig. 2 *E* and *F* and *SI Appendix, Fig. S4C*). Together, these data demonstrate that the extent of MALT1-induced Roquin cleavage correlates with TCR signal strength and target derepression. Targets with low avidity binding sites like Ox40 are derepressed at weaker and those with high functional avidity like IκB_{NS} at higher TCR signal strength.

Roquin Loss of Function and High TCR Signal Strength Promote Th17 Fate Decisions. Since the high-affinity Roquin-1 target *Nfkbid*/IκB_{NS} plays a prominent role in Th17 differentiation (42), we hypothesized that increasing inactivation of the Roquin system by conditional gene targeting could differentially affect T helper cell fate decisions. To test this, we combined the *Cd4-Cre* transgene with different combinations of floxed and wild-type alleles of *Rc3h1* and *Rc3h2* to gradually decrease Roquin expression as confirmed in immunoblots (Fig. 3*A*), using a monoclonal antibody (3F12) that detects Roquin-1 and Roquin-2 equally well (*SI Appendix, Fig. S5*). Since both paralogs act redundantly in T cells (13), this genetic titration allowed us to test the effect of decreasing Roquin activity on target derepression and T cell differentiation. Consistent with *Tnfrsf4* (Ox40) being a lower affinity target than *Nfkbid* mRNA (encoding for IκB_{NS}), we found full derepression of Ox40 levels already upon genetic inactivation of Roquin-1 encoding alleles, while IκB_{NS} became increasingly derepressed (Fig. 3 *B* and *C*). In fact, derepression of IκB_{NS} was gradual and only fully observed upon combined ablation of Roquin-1 and Roquin-2 encoding alleles (Fig. 3 *A* and *B*). Targets like ICOS, IRF4, and Regnase-1, which also promote Th17 differentiation, were derepressed in a manner more similar to *Nfkbid*/IκB_{NS} than *Tnfrsf4*/Ox40

(*SI Appendix, Fig. S6A*). Testing Th1 vs. Th17 cell differentiation, we observed that partial or complete inactivation of the system did not significantly affect the frequencies of IFNγ-producing cells under Th1 culture conditions (*SI Appendix, Fig. S6B*). Also, heterozygosity of floxed alleles for both paralogs did not enhance Th17 cell differentiation (Fig. 3 *D* and *E*). However, complete inactivation of the system strongly facilitated the development of IL-17A-producing T cells, and the expression of only one *Rc3h2* wild-type allele encoding for Roquin-2, which was determined to be lower expressed in CD4⁺ T cells than Roquin-1 (13) (Fig. 3*A*), already greatly diminished this effect (Fig. 3 *D* and *E*). We then analyzed whether Th1 and Th17 commitment also reacted differentially to antigen availability. Indeed, when cocultured with OVA₃₂₃₋₃₃₉-loaded BMDCs, full differentiation of naive OT-II cells into Th1 cells was achieved already at low (0.1 μg/mL) peptide loading concentrations (*SI Appendix, Fig. S6C*), while Th17 differentiation occurred only at much higher antigen concentrations (1–10 μg/mL) (Fig. 3 *F* and *G*). This pattern of differentiation correlated with the expression of the Th1-defining transcription factor T-bet at lower and the Th17 subset-defining transcription factor RORγt at higher antigen concentrations (*SI Appendix, Fig. S6D*). These data show how decreased Roquin activity facilitates Th17 differentiation but does not increase Th1 differentiation under Th1 polarizing conditions.

Th17 Differentiation Requires Roquin-1 Cleavage and IκB_{NS} Derepression. We then aimed to find out whether Th17 differentiation required the TCR-induced cleavage of Roquin-1 by MALT1. To answer this question, we cultured naive CD4⁺ T cells from homozygous *Rc3h1*^{Mins/Mins} as well as heterozygous and WT genotypes under Th1 or Th17 skewing conditions and analyzed IL-17A and IFN-γ production after P/I restimulation. MALT1-insensitive Roquin-1 had no effect on the frequency of IFNγ-producing T cells cultured under Th1 conditions (*SI Appendix, Fig. S7A*). However, the frequency of IL-17A-producing cells gradually decreased in heterozygous and homozygous *Rc3h1*^{Mins/Mins} as compared to wild-type mice (Fig. 3 *H* and *I*). Analyzing Th1 vs. Th17 differentiation of CD4⁺ T cells from *Rc3h1*^{Mins/Mins} in more detail, we found a trend toward less proliferation under Th17 and significantly less proliferation under Th1 differentiation conditions (*SI Appendix, Fig. S7B*). There was no difference in cell death (*SI Appendix, Fig. S7C*) and no difference of T-bet under Th1 but strongly reduced RORγt expression under Th17 differentiation conditions in CD4⁺ T cells from *Rc3h1*^{Mins/Mins} as compared to control cells (*SI Appendix, Fig. S7D*). Importantly, the decreased differentiation into Th17 cells did not promote the reciprocal Treg cell differentiation program as tested under iTreg conditions (*SI Appendix, Fig. S8A*). We also investigated the importance of Roquin-1 cleavage for Th1 vs. Tfh fate decisions. However, differentiation into the Th17 cell fate appeared more sensitive to Roquin cleavage, since adoptive transfer of SMARTA TCR transgenic CD4⁺ T cells from WT or *Rc3h1*^{Mins/Mins}, followed by subsequent LCMV Armstrong infection did not alter Tfh vs. Th1 differentiation choices significantly. Eight days post infection, we found only a tendency of slightly more Tfh (CXCR5⁺; PSGL1⁻) and less Th1 (CXCR5⁺; PSGL1⁺) differentiation in *Rc3h1*^{Mins/Mins} compared to wild-type SM(tg) T cells (*SI Appendix, Fig. S8B*).

We then asked how inactivation of the MALT1 paracaspase affected Th1/Th17 differentiation by analyzing naive CD4⁺ T differentiation from WT, *Malt1*^{+/-} and *Malt1*^{PM/-} mice. Similar to naive T cells expressing cleavage-resistant Roquin-1, T cells with inactive MALT1 paracaspase showed very similar Th1 but strongly reduced Th17 differentiation (*SI Appendix, Fig. S8C* and Fig. 3 *J* and *K*). Finally, we determined the contribution of



heterozygous or homozygous deletion of $I\kappa B_{NS}$ encoding $Nf\kappa bid^{fl/fl}$ alleles with $Cd4-Cre$. Complete inactivation of $I\kappa B_{NS}$ strongly decreased the potential of naive $CD4^+$ T cells to commit to Th17 differentiation and heterozygosity already caused a significant reduction (Fig. 3 *L* and *M*). Consistent with the greater importance for Th17 differentiation, we detected stronger cleavage of Roquin and $I\kappa B_{NS}$ expression under Th17 as compared to Th1 differentiation conditions (SI Appendix, Fig. S8D).

Together, these data show that specifically Th17 differentiation depends on MALT1-mediated cleavage of Roquin-1, and this dependency can be explained by the corresponding upregulation and increased activity of the Roquin-1 target $I\kappa B_{NS}$.

MALT1-insensitive Roquin-1 Protects from Experimental Autoimmune Encephalomyelitis. We then analyzed how induction of experimental autoimmune encephalomyelitis (EAE) that relies

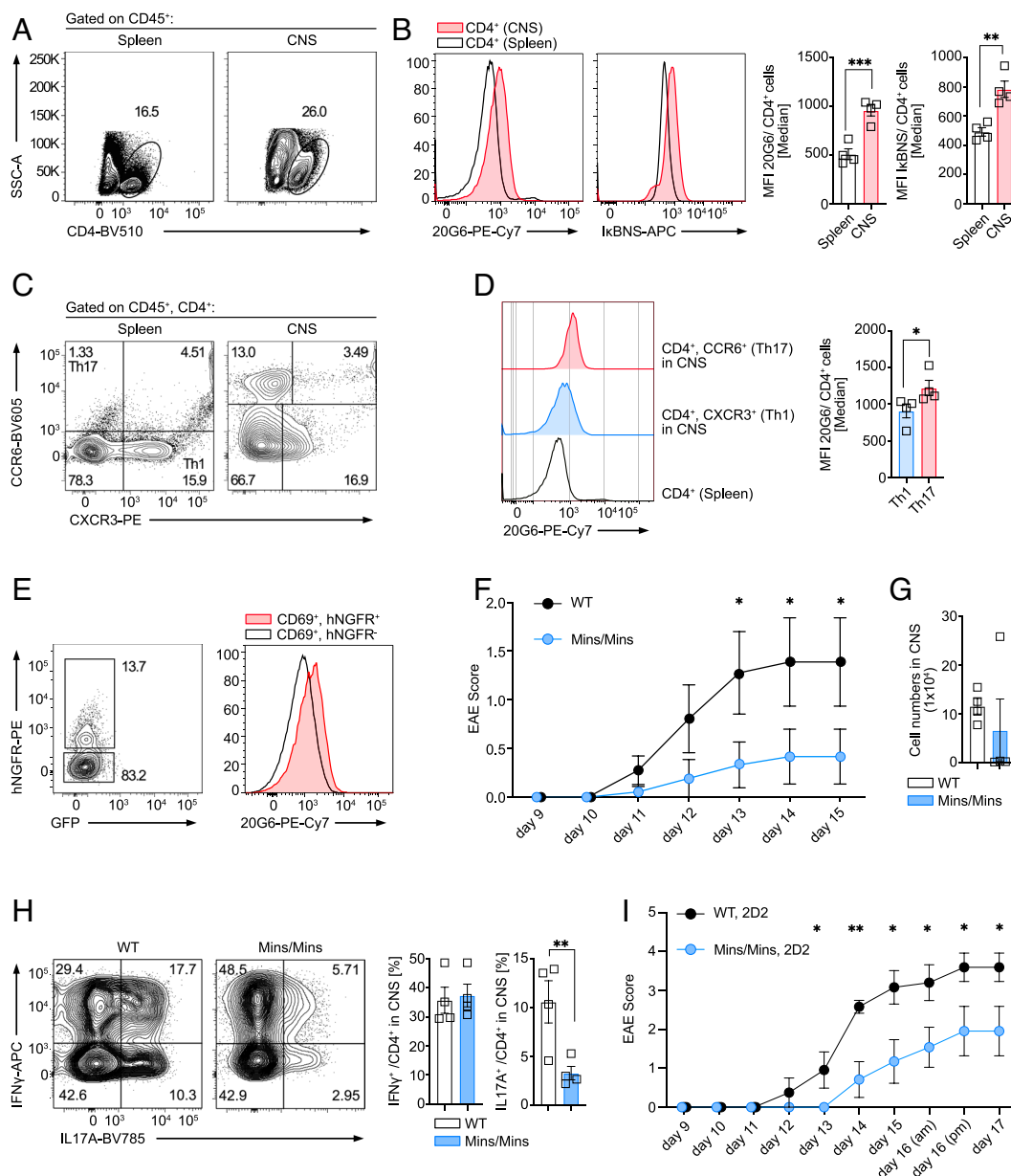


Fig. 4. Malt1-insensitive Roquin-1 protects from experimentally induced autoimmune encephalomyelitis. (A–D) WT or (E) *IL17A* reporter mice were immunized with MOG peptide in complete Freund's adjuvant (s.c.) and injected with Pertussis toxin (PTX, i.v.) on day 0 and day 2. On the peak of EAE, mice were killed, and Roquin cleavage and/or $I\kappa B_{NS}$ expression were assessed. (A) Representative plots of $CD4^+$ T cells in spleens and CNS of immunized mice. (B) Representative plots and quantifications of Roquin cleavage and $I\kappa B_{NS}$ expression in $CD4^+$ T cells from CNS (red) and spleen (black) ($n = 4$). (C) Representative plots and quantifications of CCR6⁺ (Th17) and CXCR3⁺ (Th1) $CD4^+$ T cells from spleens and CNS of immunized mice. (D) Representative plots and quantification of Roquin cleavage in Th17 vs. Th1 cells in the CNS ($n = 4$). Data are presented as mean \pm SEM. Statistical analysis was performed using an unpaired Student's *t* test, one-tailed. (E) Roquin cleavage in $hNGFR^+$ (i.e., IL17A producing) or $hNGFR^-$ $CD4^+$ T cells in the CNS of mice at the peak of EAE ($n = 4$). (F) Average clinical EAE scores from day 9 to day 15 of WT and Mins/Mins mice immunized with MOG peptide as described in (A–C). (G) Quantification of total numbers of CNS-infiltrating $CD4^+$ T lymphocytes in WT and Mins/Mins mice at day 15 (peak) of EAE isolated from spinal cords and brains (pooled per mouse) ($n = 4$). (H) Representative plots and quantifications of cytokine production by CNS infiltrating $CD4^+$ T cells of WT and Mins/Mins mice at day 15 (peak) of EAE after 4 h of restimulation with P/I. (I) Naive $CD4^+$ T cells from WT; 2D2 or Mins/Mins; 2D2 mice were adoptively transferred into $Rag1^{-/-}$ recipients, and EAE was induced as described in (A–C). Average clinical EAE scores from day 9 to day 15 ($n = 7$). CNS: central nervous system, MFI: median fluorescence intensity, P/I: PMA/Ionomycin. Data are presented as mean \pm SEM. Statistical analysis was performed using an unpaired Student's *t* test, one-tailed, for each time point. * $P < 0.05$, ** $P < 0.01$, *** $P < 0.001$, and **** $P < 0.0001$.

on Th17 responses in the central nervous system (CNS) of mice involves cleavage of Roquin. At the peak of MOG-induced EAE, CD45⁺ CD4⁺ T cells were detected in the CNS (Fig. 4A). Consistent with the accumulation of antigen-specific T cells in the CNS, we detected stronger cleavage of Roquin as well as enhanced expression of IκB_{NS} T cells in the CNS as compared to the spleen (Fig. 4B). We discriminated Th1 and Th17 cells by staining for CXCR3 and CCR6 chemokine receptors, respectively (43) (Fig. 4C). Indeed, comparing both subsets of CNS localized effector cells, we found increased Roquin cleavage in CCR6⁺ Th17 cells (Fig. 4D). Furthermore, we addressed this finding using an IL-17A reporter mouse, which expresses the hNGFR under the control of the cis-regulatory regions of the *IL17A* locus. Again, the results confirmed higher expression in CNS-localized IL-17A-producing hNGFR⁺ compared to hNGFR⁻ CD4⁺ T cells at the peak of EAE (Fig. 4E).

To elucidate whether Th17 responses were affected by Roquin cleavage in vivo, we challenged *Rc3h1*^{Mins/Mins} mice and wild-type counterparts with MOG₍₃₅₋₅₅₎ peptide in complete Freund's adjuvant to induce active EAE. We observed a reduced average clinical score in *Rc3h1*^{Mins/Mins} compared to wild-type mice when following both groups for 15 d after MOG immunization (Fig. 4F). Analyzing the CNS from selected mice of both groups that showed signs of disease (Fig. 4G and H), we found a variable amount of infiltrated CD4⁺ T cells (Fig. 4G), which, upon ex vivo stimulation with P/I, showed similar frequencies of IFNγ positive cells (Fig. 4H). However, in contrast to wild-type T cells, *Rc3h1*^{Mins/Mins} CD4⁺ T cells from the CNS were not able to produce high amounts of IL-17 or IL-17 and IFNγ, and much fewer cells produced IL-17 (Fig. 4H). Further support for the inability of *Rc3h1*^{Mins/Mins} CD4⁺ T cells to differentiate into Th17 cells was obtained by demonstrating a greatly attenuated RORγt expression in CD4⁺ T cells isolated from the inflamed CNS (SI Appendix, Fig. S8E). To analyze whether the protection of *Rc3h1*^{Mins/Mins} from EAE is a T cell-intrinsic phenotype, we generated *Rc3h1*^{Mins/Mins}; 2D2 transgenic mice, transferred 2D2 T cells of either genotype into *Rag1*^{-/-} mice, and immunized the host mice with MOG peptide. Here, *Rc3h1*^{Mins/Mins} 2D2 T cells were significantly less efficient in inducing EAE than their 2D2 wild-type counterparts, proving that cleavage-resistant Roquin-1 in T cells is responsible for protection from EAE in *Rc3h1*^{Mins/Mins} mice (Fig. 4I).

These findings reveal the physiologic importance of TCR-induced and MALT1-executed cleavage of Roquin for the development of autoimmune disease. In summary, our data promote a concept in which the TCR signal strength is correlated with the degree of Roquin inactivation. Exceeding a specific threshold enables sufficient induction of IκB_{NS} expression as a prerequisite for Th17 cell differentiation in vitro and in vivo.

Discussion

There is growing therapeutic interest in manipulating MALT1, and inhibitors of the MALT1 paracaspase are currently investigated in clinical trials. The therapeutic aims are to deprive hematologic tumor cells from an essential growth signal or to modulate the balance of Treg and conventional T cells in antitumor immunity (44). Preclinical studies have also studied inactivation of the MALT1 targets Roquin-1/2 or Regnase-1 or inhibition of Roquin-1/Regnase-1 cooperation in tumor-specific T cells or CAR T cells (40, 45–48). For the success and safety of these approaches, we now need a comprehensive understanding of the function and regulation of these factors in the different cell types.

In this study, we define the molecular and cellular consequences of selectively inhibiting Roquin-1 cleavage by MALT1. We identify a major role for Roquin-1 cleavage in the phenotype of mice

expressing a constitutively active MALT1 paracaspase (7). We propose that the autoimmune/autoinflammatory phenotype of these mice results from constitutive cleavage and thereby loss-of-function of Roquin-1, which triggers activation of naive T cells as well as their differentiation into effector cells. Indeed, acute loss-of-function of Roquin-1 and Roquin-2 proteins is associated with spontaneous CD4⁺ and CD8⁺ T cell activation, as well as preferential Tfh and Th17 differentiation (40). From this work, it becomes clear that T cell quiescence is not primarily defined by the absence of foreign antigen recognition, but rather requires the TRAF6/MALT1 interaction and high Roquin activity to maintain naive T cells constantly exposed to tonic TCR signals, in a quiescent state. The Roquin-1-regulated targets that control T cell quiescence are currently unknown, and it will be interesting to find out whether they include poised mRNAs, which are kept untranslated until the naive T cell recognizes antigen (49, 50). Unfortunately, the mortality of *Malt1*^{TBM/TBM} mice during adolescence precludes a detailed analysis of T helper cell differentiation. Nevertheless, Tfh and Th17 responses likely contribute to the observed phenotype since elevated autoantibodies and T helper cell cytokines are present in the sera of these mice (7). Apparently, this development of autoimmunity occurs in the absence of TCR/TRAF6/MALT1-induced NF-κB activity (7) but may involve the activation of NF-κB through other surface receptors like Ox40, which is controlled by Roquin proteins (13, 22). Several targets of Roquin have been determined to have a role in Tfh and Th17 differentiation. The hypomorphic *sanroque* allele of *Rc3h1* (encoding for Roquin-1^{san}) exhibits an accumulation of Tfh and Th1 effector cells (11, 12, 51). In contrast, combined deletion of Roquin-1 and Roquin-2 encoding alleles in peripheral T cells promotes Tfh and Th17 differentiation (4). Interestingly, we did not detect significant differences in Th1 vs. Tfh cell fate decisions in LCMV Armstrong infections in T cells from mice expressing MALT1-insensitive Roquin-1. These findings could suggest that Tfh and Th1 fate decisions may not be different in their dependence on the expression of high-affinity targets of Roquin-1. Instead, we show that Th17 cell fate decisions depend on the cleavage of Roquin-1 by MALT1. Our mouse model of MALT1-insensitive Roquin-1 (*Rc3h1*^{Mins/Mins}) suggests that repression of IκB_{NS} (*Nfkbid*) by Roquin-1 is a major mechanism for integrating TCR signaling into Th17 differentiation. This conclusion is further supported by the graded conditional inactivation of the Roquin-1 and Roquin-2 encoding alleles in T cells. Only their complete inactivation led to full derepression of IκB_{NS} and full Th17 differentiation. Moreover, *Rc3h1*^{Mins/+} and *Rc3h1*^{Mins/Mins} genotypes limited IκB_{NS} upregulation during activation of CD4⁺ T cells, and *Rc3h1*^{Mins/Mins} mice showed impaired Th17 differentiation in vitro as well as in vivo during EAE. Low levels of IκB_{NS} in *Rc3h1*^{Mins/Mins} mice can explain the reduced Th17 differentiation as we also found a comparable impairment in the heterozygous *Nfkbid*^{fl/+}; *Cd4-Cre* as well as an even more pronounced reduction of Th17 differentiation in the *Nfkbid*^{fl/fl}; *Cd4-Cre* genotype. Only antigen signals of high strength induced the extensive cleavage of Roquin that was required for full upregulation of IκB_{NS}, which did not affect Th1 but was necessary for Th17 differentiation and experimental induction of Th17-driven autoimmunity. The functional avidity of the *Nfkbid* mRNA for Roquin binding involves on the one hand the high affinity of individual binding sites of the CDE and ADE type and on the other hand the high number of at least seven Roquin-recognized stem-loops and LBEs in its 3'-UTR (14, 15). These binding sites have been proposed to serve accessory, redundant, or cooperative functions and confer induced *Nfkbid* mRNA decay and also translational inhibition of IκB_{NS} (14). Translational inhibition affects only a subset of Roquin targets, which are enriched in four or more Roquin binding sites (14). Of course, also other high or intermediate affinity targets like

Nfkbiz, *Irf4*, and *Icos* may, following their derepression at intermediate or high TCR strength, additionally promote Th17 commitment (42, 52–55). Conversely, also the low avidity target Ox40 can shape this program further since Ox40 was demonstrated to inhibit Th17 differentiation via activation of noncanonical NF- κ B signaling and RelB-mediated recruitment of epigenetic repressors to the *Il17* locus (56). In our experiments Ox40 was already fully induced at low TCR signal strength or intermediate levels of Roquin inactivation and could inhibit Th17 commitment in response to T cell stimulations that induce suboptimal $\text{I}\kappa\text{B}_{\text{NS}}$ levels. Together, we propose that the MALT1/Roquin/ $\text{I}\kappa\text{B}_{\text{NS}}$ axis establishes a unique post-transcriptional threshold of TCR strength in Th17 differentiation since blocking Roquin-1 cleavage by MALT1 did not shift the cells toward iTreg differentiation as it was previously observed for TCR strength- and Itk-dependent control of Th17 differentiation (31, 57).

Here, we describe a mouse model that genetically renders one substrate of MALT1 insensitive to proteolytic cleavage. These *Rc3h1*^{Mins/Mins} mice shared some phenotypes with *Malt1*^{PM/PM} mice including a milder reduction in thymic Treg frequencies (8–10) and to a similar extent an impairment of Th17 differentiation (8). At present, it is possible that the system is even more strongly involved than evident from *Rc3h1*^{Mins/Mins} mice, since the lack of Roquin-1 cleavage may also be compensated by cleavage of the functionally redundant Roquin-2 or potentially through cleavage of the functionally cooperating Regnase-1 protein. Future work will answer these questions by generating MALT1-insensitive Roquin-2 (*Rc3h2*) or Regnase-1 alleles and by combining them with *Rc3h1*^{Mins/Mins} alleles. Of note, targets of MALT1 in the NF- κ B or other pathways could also be crucial for the phenotypes of *Malt1*^{PM/PM} mice that are not shared in *Rc3h1*^{Mins/Mins} mice (58, 59).

Importantly, our mouse model reveals the impact of the MALT1 protease activity on Th17 differentiation and Th17-driven autoimmunity segregates with cleavage of the Roquin-1 substrate. In active EAE, we detect stronger cleavage of Roquin in CNS-localized CD4⁺ T cells that produce IL-17A compared with CNS-localized CD4⁺ cells that are negative for IL-17A expression. This finding prompts the question of whether chronically activated pathogenic CD4⁺ T cells in Th17-related diseases in general show accumulation of MALT1-cleaved Roquin. Future research needs to evaluate MALT1-mediated Roquin cleavage as a biomarker and targeting of MALT1 paracaspase activity in Th17-driven diseases.

Materials and Methods

Animals. All experiments involving mice and rats were performed in accordance with the regulations and with approval by the local government (Regierung von Oberbayern, ROB). Mice and rats were housed in specific pathogen-free barrier facilities in standard cages on a 12-h light/dark cycle with ad libitum access to food and water in accordance with institutional, state, and federal guidelines of the Helmholtz Zentrum München and the Ludwig-Maximilians-Universität München.

T Cell Cultures. For in vitro cultivation of primary murine CD4⁺ T cells, single-cell suspensions in T cell isolation buffer (PBS supplemented with 2% FCS and 1 mM EDTA) were generated from spleens and peripheral lymph nodes. Erythrocytes were lysed using a TAC-lysis buffer (13 mM Tris and 140 mM NH₄Cl, pH 7.2). CD4⁺ T cells were isolated using the negative selection EasySep™ Mouse CD4⁺ T cell isolation Kit (STEMCELL). A total of 4–5 × 10⁶ T cells were activated in vitro in 6-well plates by plate-bound and goat anti-hamster IgG-cross-linked (MP Biomedicals, #56984) anti-CD3 (0.25 μg/mL; clone 2C11, in-house) and anti-CD28 antibodies (2.5 μg/mL; clone 37.5 N, in-house). Cells were cultured for 6 d in T cell medium (DMEM medium (Gibco) supplemented with 10% FCS, 10 units/mL penicillin, 10 μg/mL streptomycin (both ThermoFisher), 10 mM HEPES (Gibco), 50 μM β-mercaptoethanol (β-ME; Invitrogen), 1x nonessential amino acids (NEAAs; Gibco), and 200 units/mL hIL-2 (Novartis)) under Th1-polarizing conditions (10 μg/mL

anti-IL-4 (clone 11B11, in-house) and 10 ng/mL IL-12 (BD Pharmingen)). Naive CD4⁺ T cells were isolated using the EasySep™ Mouse Naive CD4⁺ T cell isolation Kit (STEMCELL). For anti-CD3 titrations with constant anti-CD28, total CD3⁺ T cells were isolated and cultured on 96-well U-bottom plates with plate-bound anti-CD3 and anti-CD28 concentrations for 18 h. T cells were maintained in T cell medium (RPMI 1640 + GlutaMAX (Gibco) supplemented with 10% FCS, 10 units/mL penicillin (ThermoFisher), 10 μg/mL streptomycin (ThermoFisher), 5 μM β-mercaptoethanol (β-ME; Invitrogen) and 5 ng/mL IL-7 (ImmunoTools) (Fig. 2A, *SI Appendix*, Fig. S3).

Cocultures. Bone marrow (BM) cells from the tibia and femur of wild-type mice were differentiated to mature BM-derived dendritic cells (BMDCs) for 6 d in T cell medium supplemented with 20 ng/mL GM-CSF (Cell Signaling Technologies) and kept at 37 °C 5% CO₂. On day 6 of differentiation, lipopolysaccharide (LPS, 100 ng/mL, Sigma) was added for a 24 h to induce maturation of BMDCs, and full maturation was confirmed by surface CD11c and MHCI expression. Mature BMDCs were loaded with different concentrations of Ovalbumin peptides, OVA_{323–339} (wild type or R9 mutant; BIO TREND), for 2–3 h at 37 °C 5% CO₂, and cocultured with naive CD4⁺ OTII-T cells at a 1:1 ratio.

For mixed lymphocyte stimulations, 50,000 naive CD4⁺ OTII-TCR-transgenic T cells were cocultured with 50,000 congenically marked splenocytes loaded with different OVA peptides. Cells were supplemented with 5 ng/mL murine IL-7 (ImmunoTools) and kept at 37 °C for 18 h (*SI Appendix*, Fig. S3E).

In Vitro Differentiation of Naive CD4⁺ T Cells. A total of 200,000 naive CD4⁺ T cells were cultured in 96-well flat bottom plates for 3.5 d under T_H0 (no cytokines and no blocking antibodies), Th1 (10 μg/mL anti-IL-4 and 10 ng/mL IL-12), Th17 (10 μg/mL anti-IL-4, 10 μg/mL anti-IL-12, 10 ng/mL TGFβ, 60 ng/mL IL-6, and 5 μg/mL anti-IFNγ), or iTreg (10 ng/mL TGFβ, 10 μg/mL anti-IL-4, and 5 μg/mL anti-IFNγ) polarizing conditions. On day 2 of differentiation, cells were split 1:2 by adding T cell medium without additional cytokines. Differentiated cells were washed with cold PBS and subsequently stimulated for 5 h with 20 nM PMA and 1 μM ionomycin. After 2.5 h, 10 μg/mL brefeldin A (BrdA) was added.

Immunophenotyping. Single-cell suspensions of isolated lymphocytes were stained for viability [Fixable Viability dye (eF780) or LIVE/DEAD Fixable Blue (Invitrogen)], followed by surface staining for 20 min protected from light at 4 °C. Cells were fixed in 2% formaldehyde (FA) for cytokine staining or 4% PFA for 20G6 staining for 15 min at RT. For transcription factor staining, cells were fixed in Foxp3 Fix/Perm buffer (Invitrogen) for 20 min at 4 °C.

Intracellular stainings with in-house hybridoma supernatant antibodies or directly conjugated commercial antibodies were performed after fixation and permeabilization in (0.5% Saponin, 1.0% BSA, PBS) or Foxp3 staining kit permeabilization buffer (Invivogen) for 40 min at 4 °C and washed with FACS buffer. Flow cytometry data were acquired with BD LSRFortessa (5-laser), the BD FACSCanto (3-laser), or the Cytoflex S (4-laser, Beckman Coulter) flow cytometers.

LCMV Infection of Mice. LCMV Armstrong virus was propagated in Baby hamster kidney-21 cells (BHK-21). Virus titers were determined by plaque assays on Vero cells as described previously (60). To assess T cell-intrinsic Tfh vs. Th1 differentiation, 1 × 10⁴ SMARTA TCR-tg (SM(tg)), *Rc3h1*^{+/+} or SM(tg); *Rc3h1*^{Mins/Mins} CD4⁺ T cells were adoptively transferred into congenically marked CD45.1 WT recipients. One day after transfer, recipient mice were infected with 2 × 10⁵ pfu LCMV Armstrong intraperitoneally (i.p.) and killed 8 d postinfection (dpi).

Experimental Autoimmune Encephalomyelitis (EAE). The active EAE disease model was induced on day 0 by subcutaneous (s.c.) injection of 200 μg MOG peptide (Auspep Pty Ltd.) emulsified in CFA (BD Difco™ Adjuvants) at the tail base of age-matched mice. 100 ng of pertussis toxin (PTX, in PBS; Sigma) was intravenously (i.v.) injected on day 0 and on day 2 (200 ng total dose). Mice were checked on a daily basis and scored starting at day 9 after MOG/CFA and PTX injections. Clinical scores were documented up until day 15 after induction resembling the peak of disease scores in wild-type counterparts.

To induce EAE in a T cell conditional Mins/Mins setting, 1,500 CD4⁺, CD25⁻ T cells from 2D2-TCR transgenic *Rc3h1*^{+/+} or *Rc3h1*^{Mins/Mins} mice were injected into *Rag1*^{-/-} recipients. EAE was induced as described above.

On day 15, mice were killed by isoflurane inhalation, perfused with PBS and CNS samples from spinal cords and brains were isolated for ex vivo analysis of

T cells. Briefly, CNS tissue was cut into small pieces and digested by incubation with 1 mg/mL DNase I (Sigma) and 2.5 mg/mL collagenase D (Sigma) in DMEM medium supplemented with 10% FCS, 10 units/mL penicillin, 10 µg/mL streptomycin, 10 mM HEPES, 50 µM β-ME, and 1x NEAAs for 90 min at 37 °C. CNS-infiltrating mononuclear cells were isolated by Percoll gradient centrifugation (37%, 70% Percoll in PBS buffer; GE Healthcare).

Western Blotting. T cells were washed in ice-cold PBS were subsequently lysed in 20 mM Tris-HCl, pH 7.5, 150 mM NaCl, 0.25% (v/v) NP-40, 1.5 mM MgCl₂, 1 mM DTT supplemented with 1x cOmplete, EDTA-free Protease Inhibitor Cocktail (Roche) for 15 min on ice (4 °C). Lysates were clarified for 15 min at 10,000×g, and protein concentration was determined by Bradford assay (Bio-Rad). Equal amounts of protein lysates (30–50 µg) were denatured at 95 °C for 5 min in 4 × Laemmli buffer (314 mM Tris, 50% glycerol, 5% SDS, 5% β-mercaptoethanol, and 0.01% bromophenol blue, pH 6.8), size-separated by SDS-PAGE, transferred to a MeOH-activated PVDF membrane, and incubated with respective primary and HRP-conjugated secondary antibodies (CST). Signal detection was performed with ECL western blotting reagents (Novex Invitrogen, Amersham GE or in-house produced ECL) and DV-B medical X-ray films.

Detailed information on methods and results is also available at ref. 61 and https://edoc.ub.uni-muenchen.de/292777/Schmidt_Henrik.pdf.

Data, Materials, and Software Availability. All study data are included in the article and/or *SI Appendix*.

ACKNOWLEDGMENTS. We thank Lena Esser, Christina Baumann, Andrew Flatley, and Sabrina Schumann for excellent technical support. We acknowledge the Core Facility Flow Cytometry at the Biomedical Center, Ludwig-Maximilians-Universität

München, for providing equipment. The work was supported by the German Research Foundation grants SPP-1935 #313381103 (to V.H.), SFB-1054 projects A03 #210592381 (to V.H.), A04 (to D.K.), B01 (to J.R.) and B06 (to T.K.), TRR338 #452881907 (to V.H.), TRR355 #490846870 A06 to V.H. and B07 to T.K., HE335977-1 #432656284 and HE335978-1 #444891219 to V.H., and TR128-A07, TR274-A01 and EXC 2145 (SyNergy) #390857198 to T.K. as well as grants from the Wilhelm Sander, Fritz Thyssen, Else Kröner-Fresenius and Deutsche Krebshilfe foundations to V.H., and the ERC (CoG 647215) to T.K. The study was also funded by the German Research Foundation grants SFB-854 project A23 and SCHM1586/6-2 to I.S.

Author affiliations: ^aInstitute for Immunology, Medical Faculty, Biomedical Center, Ludwig-Maximilians-Universität München, Planegg-Martinsried 82152, Germany; ^bResearch Unit Signaling and Translation, Molecular Targets and Therapeutics Center, Helmholtz Zentrum München, German Research Center for Environmental Health, Neuherberg 85764, Germany; ^cInstitute for Experimental Neuroimmunology, Technical University of Munich, School of Medicine, Munich 81675, Germany; ^dInstitute of Developmental Genetics, Helmholtz Zentrum München, German Research Center for Environmental Health, Neuherberg 85764, Germany; ^eResearch Unit Molecular Immune Regulation, Molecular Targets and Therapeutics Center, Helmholtz Zentrum München, German Research Center for Environmental Health, Munich 81337, Germany; ^fMonoclonal Antibody Core Facility, Helmholtz Zentrum München, German Research Center for Environmental Health, Neuherberg 85764, Germany; ^gDepartment of Molecular Immunology, ZKF2, Ruhr-University Bochum, Bochum 44801, Germany; ^hInstitute of Structural Biology, Molecular Targets and Therapeutics Center, Helmholtz Zentrum München, German Research Center for Environmental Health, Neuherberg 85764, Germany; ⁱTranslaTUM, Center for Translational Cancer Research, Technical University of Munich, Munich 81675, Germany; ^jInstitute of Clinical Chemistry and Pathobiochemistry, School of Medicine, Technical University of Munich, Munich 81675, Germany; ^kMax-Planck-Institute of Psychiatry, Munich 80804, Germany; ^lChair of Developmental Genetics, TUM School of Life Sciences, Technische Universität München, Freising 85354, Germany; and ^mMunich Cluster for Systems Neurology, Munich 81377, Germany

1. J. Ruland, L. Hartjes, CARD-BCL-10-MALT1 signalling in protective and pathological immunity. *Nat. Rev. Immunol.* **19**, 118–134 (2019).
2. B. Coornaert *et al.*, T cell antigen receptor stimulation induces MALT1 paracaspase-mediated cleavage of the NF-κappaB inhibitor IκB. *Nat. Immunol.* **9**, 263–271 (2008).
3. P. A. Bell *et al.*, Integrating knowledge of protein sequence with protein function for the prediction and validation of new MALT1 substrates. *Comput. Struct. Biotechnol. J.* **20**, 4717–4732 (2022).
4. K. M. Jeltsch *et al.*, Cleavage of roiquin and regnase-1 by the paracaspase MALT1 releases their cooperatively repressed targets to promote TH17 differentiation. *Nat. Immunol.* **15**, 1079–1089 (2014).
5. T. Uehata *et al.*, Malt1-induced cleavage of regnase-1 in CD4(+) helper T cells regulates immune activation. *Cell* **153**, 1036–1049 (2013).
6. D. Yamasoba *et al.*, N4BP1 restricts HIV-1 and its inactivation by MALT1 promotes viral reactivation. *Nat. Microbiol.* **4**, 1532–1544 (2019).
7. T. J. O'Neill *et al.*, TRAF6 prevents fatal inflammation by homeostatic suppression of MALT1 protease. *Sci. Immunol.* **6**, eabh2095 (2021).
8. F. Bornancin *et al.*, Deficiency of MALT1 paracaspase activity results in unbalanced regulatory and effector T and B cell responses leading to multiorgan inflammation. *J. Immunol.* **194**, 3723–3734 (2015).
9. A. Gewies *et al.*, Uncoupling Malt1 threshold function from paracaspase activity results in destructive autoimmune inflammation. *Cell Rep.* **9**, 1292–1305 (2014).
10. M. Jaworski *et al.*, Malt1 protease inactivation efficiently dampens immune responses but causes spontaneous autoimmunity. *EMBO J.* **33**, 2765–2781 (2014).
11. S. J. Tavernier *et al.*, A human immune dysregulation syndrome characterized by severe hyperinflammation with a homozygous nonsense Roquin-1 mutation. *Nat. Commun.* **10**, 4779 (2019).
12. C. G. Vinuesa *et al.*, A RING-type ubiquitin ligase family member required to repress follicular helper T cells and autoimmunity. *Nature* **435**, 452–458 (2005).
13. K. U. Vogel *et al.*, Roquin paralogs 1 and 2 redundantly repress the Icos and Oxo40 costimulator mRNAs and control follicular helper T cell differentiation. *Immunity* **38**, 655–668 (2013).
14. K. Essig *et al.*, Roquin targets mRNAs in a 3'-UTR-specific manner by different modes of regulation. *Nat. Commun.* **9**, 3810 (2018).
15. K. Leppke *et al.*, Roquin promotes constitutive mRNA decay via a conserved class of stem-loop recognition motifs. *Cell* **153**, 869–881 (2013).
16. D. Yu *et al.*, Roquin represses autoimmunity by limiting inducible T-cell co-stimulator messenger RNA. *Nature* **450**, 299–303 (2007).
17. S. Sakurai, U. Ohto, T. Shimizu, Structure of human Roquin-2 and its complex with constitutive-decay element RNA. *Acta Crystallogr. F. Struct. Biol. Commun.* **71**, 1048–1054 (2015).
18. A. Schlundt *et al.*, Structural basis for RNA recognition in roquin-mediated post-transcriptional gene regulation. *Nat. Struct. Mol. Biol.* **21**, 671–678 (2014).
19. A. Schuetz, Y. Murakawa, E. Rosenbaum, M. Landthaler, U. Heinemann, Roquin binding to target mRNAs involves a winged helix-turn-helix motif. *Nat. Commun.* **5**, 5701 (2014).
20. M. Srivastava *et al.*, Roquin binds microRNA-146a and Argonaute2 to regulate microRNA homeostasis. *Nat. Commun.* **6**, 6253 (2015).
21. D. Tan, M. Zhou, M. Kiledjian, L. Tong, The ROO domain of Roquin recognizes mRNA constitutive-decay element and double-stranded RNA. *Nat. Struct. Mol. Biol.* **21**, 679–685 (2014).
22. R. Janowski *et al.*, Roquin recognizes a non-canonical hexaloop structure in the 3'-UTR of Oxo40. *Nat. Commun.* **7**, 11032 (2016).
23. Y. Murakawa *et al.*, RC3H1 post-transcriptionally regulates A20 mRNA and modulates the activity of the IKK/NF-κappaB pathway. *Nat. Commun.* **6**, 7367 (2015).
24. E. Glasmacher *et al.*, Roquin binds inducible costimulator mRNA and effectors of mRNA decay to induce microRNA-independent post-transcriptional repression. *Nat. Immunol.* **11**, 725–733 (2010).
25. A. Sgromo *et al.*, A CAF40-binding motif facilitates recruitment of the CCR4-NOT complex to mRNAs targeted by Drosophila Roquin. *Nat. Commun.* **8**, 14307 (2017).
26. A. Bertossi *et al.*, Loss of Roquin induces early death and immune deregulation but not autoimmunity. *J. Exp. Med.* **208**, 1749–1756 (2011).
27. K. Martin *et al.*, Malt1 protease deficiency in mice disrupts immune homeostasis at environmental barriers and drives systemic T cell-mediated autoimmunity. *J. Immunol.* **203**, 2791–2806 (2019).
28. M. Rosenbaum *et al.*, Bcl10-controlled Malt1 paracaspase activity is key for the immune suppressive function of regulatory T cells. *Nat. Commun.* **10**, 2352 (2019).
29. G. Fu *et al.*, Themis sets the signal threshold for positive and negative selection in T-cell development. *Nature* **504**, 441–445 (2013).
30. H. Yamane, W. E. Paul, Early signaling events that underlie fate decisions of naive CD4(+) T cells toward distinct T-helper cell subsets. *Immunity Rev.* **252**, 12–23 (2013).
31. J. Gomez-Rodriguez *et al.*, Itk-mediated integration of T cell receptor and cytokine signaling regulates the balance between Th17 and regulatory T cells. *J. Exp. Med.* **211**, 529–543 (2014).
32. S. Keck *et al.*, Antigen affinity and antigen dose exert distinct influences on CD4-T cell differentiation. *Proc. Natl. Acad. Sci. U.S.A.* **111**, 14852–14857 (2014).
33. V. Krishnamoorthy *et al.*, The IRF4 gene regulatory module functions as a read-write integrator to dynamically coordinate T helper cell fate. *Immunity* **47**, 481–497.e487 (2017).
34. N. J. Tubo *et al.*, Single naive CD4+ T cells from a diverse repertoire produce different effector cell types during infection. *Cell* **153**, 785–796 (2013).
35. N. van Panhuys, F. Klauschen, R. N. Germain, T-cell-receptor-dependent signal intensity dominantly controls CD4(+) T cell polarization in vivo. *Immunity* **41**, 63–74 (2014).
36. A. Iwata *et al.*, Quality of TCR signaling determined by differential affinities of enhancers for the composite BAIT-IRF4 transcription factor complex. *Nat. Immunol.* **18**, 563–572 (2017).
37. Y. L. Cho *et al.*, TCR signal quality modulates fate decisions of single CD4(+) T cells in a probabilistic manner. *Cel. Rep.* **20**, 806–818 (2017).
38. J. M. Robertson, P. E. Jensen, B. D. Evavold, D011.10 and OT-II T cells recognize a C-terminal ovalbumin 323–339 epitope. *J. Immunol.* **164**, 4706–4712 (2000).
39. J. N. Tants, L. M. Becker, F. McNicoll, M. Muller-McNicoll, A. Schlundt, NMR-derived secondary structure of the full-length Oxo40 mRNA 3'UTR and its multivalent binding to the immunoregulatory RBP Roquin. *Nucleic Acids Res.* **50**, 4083–4099 (2022).
40. G. Behrens *et al.*, Disrupting Roquin-1 interaction with Regnase-1 induces autoimmunity and enhances antitumor responses. *Nat. Immunol.* **22**, 1563–1576 (2021).
41. K. P. Hoefig *et al.*, Defining the RBPome of primary T helper cells to elucidate higher-order Roquin-mediated mRNA regulation. *Nat. Commun.* **12**, 5208 (2021).
42. M. Annemann *et al.*, IκappaBNS regulates murine Th17 differentiation during gut inflammation and infection. *J. Immunol.* **194**, 2888–2898 (2015).
43. A. Reboldi *et al.*, C-C chemokine receptor 6-regulated entry of TH-17 cells into the CNS through the choroid plexus is required for the initiation of EAE. *Nat. Immunol.* **10**, 514–523 (2009).
44. T. R. Mempel, D. Krappmann, Combining precision oncology and immunotherapy by targeting the MALT1 protease. *J. Immunother. Cancer* **10**, e005442 (2022).
45. D. Mai *et al.*, Combined disruption of T cell inflammatory regulators Regnase-1 and Roquin-1 enhances antitumor activity of engineered human T cells. *Proc. Natl. Acad. Sci. U.S.A.* **120**, e2218632120 (2023).
46. J. Wei *et al.*, Targeting REGNASE-1 programs long-lived effector T cells for cancer therapy. *Nature* **576**, 471–476 (2019).

47. H. Zhao *et al.*, Genome-wide fitness gene identification reveals Roquin as a potent suppressor of CD8 T cell expansion and anti-tumor immunity. *Cell Rep.* **37**, 110083 (2021).
48. W. Zheng *et al.*, Regnase-1 suppresses TCF-1+ precursor exhausted T-cell formation to limit CAR-T-cell responses against ALL. *Blood* **138**, 122–135 (2021).
49. M. Turner, Regulation and function of poised mRNAs in lymphocytes. *Bioessays* **45**, e2200236 (2023).
50. T. Wolf *et al.*, Dynamics in protein translation sustaining T cell preparedness. *Nat. Immunol.* **21**, 927–937 (2020).
51. S. K. Lee *et al.*, Interferon-gamma excess leads to pathogenic accumulation of follicular helper T cells and germinal centers. *Immunity* **37**, 880–892 (2012).
52. A. T. Bauquet *et al.*, The costimulatory molecule ICOS regulates the expression of c-Maf and IL-21 in the development of follicular T helper cells and TH-17 cells. *Nat. Immunol.* **10**, 167–175 (2009).
53. A. Brustle *et al.*, The development of inflammatory T(H)-17 cells requires interferon-regulatory factor 4. *Nat. Immunol.* **8**, 958–966 (2007).
54. K. Okamoto *et al.*, I κ B ζ regulates T(H)17 development by cooperating with ROR nuclear receptors. *Nature* **464**, 1381–1385 (2010).
55. C. M. Paulos *et al.*, The inducible costimulator (ICOS) is critical for the development of human T(H)17 cells. *Sci. Transl. Med.* **2**, 55ra78 (2010).
56. X. Xiao *et al.*, The costimulatory receptor OX40 inhibits Interleukin-17 expression through activation of repressive chromatin remodeling pathways. *Immunity* **44**, 1271–1283 (2016).
57. J. Gomez-Rodriguez, Z. J. Kraus, P. L. Schwartzberg, Tec family kinases Itk and Rlk/Txk in T lymphocytes: Cross-regulation of cytokine production and T-cell fates. *FEBS J.* **278**, 1980–1989 (2011).
58. M. Baens *et al.*, Malt1 self-cleavage is critical for regulatory T cell homeostasis and anti-tumor immunity in mice. *Eur. J. Immunol.* **48**, 1728–1738 (2018).
59. I. Skordos *et al.*, Normal lymphocyte homeostasis and function in MALT1 protease-resistant HOIL-1 knock-in mice. *FEBS J.* **290**, 2032–2048 (2023).
60. M. Pellegrini *et al.*, IL-7 engages multiple mechanisms to overcome chronic viral infection and limit organ pathology. *Cell* **144**, 601–613 (2011).
61. H. Schmidt, "Investigating T cell receptor-dependent post-transcriptional gene regulation by Roquin to characterize lymphocyte fate decisions. Elektronische Hochschulschriften der LMU München", Dissertation, LMU München: Medizinische Fakultät (2021). https://edoc.ub.uni-muenchen.de/29277/7/Schmidt_Henrik.pdf. Accessed 11 February 2022.